sustainability

MDPI

Article

The Vegetation Dynamics and Climate Change Responses by Leaf Area Index in the Mu Us Desert

Defeng Zheng [1], Yanhui Wang [1], Yanying Shao [2,*] and Lixin Wang [3]

1 School of Urban and Environmental Science, Liaoning Normal University, Dalian 116029, China; defengzheng@lnnu.edu.cn (D.Z.); yhwang112@163.com (Y.W.)
2 Department of Geography, Changchun School Affiliated to Beijing Normal University, Changchun 130000, China
3 Jilin Yinhe Water Conservancy Hydropower New Technology Design Co., Ltd., Changchun 130000, China; lixinwang61@163.com
* Correspondence: shaoyanying@126.com

Received: 11 May 2019; Accepted: 28 May 2019; Published: 4 June 2019

check for updates

Abstract: Knowing the long-dated dynamic changes of vegetation in the Mu Us Desert is critical for strengthening sustainable management of vegetation restoration projects in the next planned cycle until 2050. To predict leaf area indexes (LAIs) under long-dated climate scenarios (2013–2050) in the Mu Us Desert, the relationship between earlier meteorological data and LAI was tracked with regression analysis on the basis of LAI data from the Global Land Surface Satellite (GLASS) and the grid meteorological data during 1982–2012, and the LAIs were estimated based on five-Global Circulation Model (GCM) ensemble means under three representative concentration pathways (RCP 2.6, RCP 4.5 and RCP 8.5). We found an increasing trend in precipitation and a significant increase in potential evapotranspiration (PET) during the earlier period in the Mu Us Desert, and that could continue into the long-dated under three RCPs in the Mu Us Desert. Warming trends occur in the earlier and long-dated periods for annual average air temperature. Compared with the observations, the temperature rises respectively by 0.6 °C, 0.7 °C, and 1 °C under the three RCPs mentioned above. The annual maximum LAI largely increased with a rate-of-change of 0.029 $m^2 \cdot m^{-2} \cdot yr^{-1}$. Precipitation has been a major influencing factor to vegetation dynamics and growth in the Mu Us Desert. The permissible LAIs by 2050 are 0.42–0.88 $m^2 \cdot m^{-2}$, 0.42–0.87 $m^2 \cdot m^{-2}$, and 0.41–0.87 $m^2 \cdot m^{-2}$ under the three RCPs, respectively. Contrasted with the baseline period (1982–2012), the LAI is found to be already close to the current value in the northwestern and southern Mu Us Desert.

Keywords: leaf area index; vegetation restoration; climatic variables; general circulation models

1. Introduction

For the terrestrial ecosystem, vegetation is an important component. Desert vegetation provides important water and soil conservation services [1] and plays a dominant role in the prevention of desertification, mitigation of wind-sand damage, and restoration of the local environment in arid and semi-arid ecosystems [2–4]. Revegetation is an important approach for restoring degraded and disturbed ecosystems resulting from inappropriate anthropogenic activities [5,6], and has been internationally recognized and accepted as one of the most reasonable and effective ways [7–10]. Some international organizations, such as UNDP, UNEP, and FAO, had implemented a series of plans in sand-fixing plants to prevent and control desertification, especially in developing countries for rebuilding desert ecosystems.

Since 1978, China has launched some of the most ambitious ecological restoration programs [11,12] called vegetation rehabilitation programs, including the Grain to Green Project [13], Natural Forest Conservation Program, and the Three North Shelter Forest System Project [14,15]. The Mu Us Desert is one of the main areas of vegetation restoration [9]. Since its implementation in 1978, artificial vegetation construction has remarkably increased in desert regions and promoted local habitat restoration [16]. However, Guo et al. showed that the soil water status gradually deteriorated with the increase of vegetation coverage [17]. Mu et al. found that large-scale artificial vegetation restoration caused excessive consumption of deep soil water and affected the sustainability of vegetation restoration [18]. Feng et al. thought vegetation expansion in water-limited desert regions would exacerbate the shortage of water resources [19]. It is a challenge as how best to recover vegetation and safeguard regional water resources safely at the same time in Mu Us Desert.

Limited efforts have focused on soil water carrying capacity for vegetation [20–22], which is associated with plot scales [22–24]. Due to the strong influences from multiple environmental controls like hydrological and climate elements, terrain, vegetation types, and soil characteristics with spatial and temporal heterogeneity at a regional scale [25], the research results from plot scales could not be directly applied to guide the ecological construction and allocate water resources optimally on a larger scale. The planned period for the next cycle ending is in 2050 [14,26,27]. However, how much vegetation is reasonable and effective for re-vegetation projects in the Mu Us Desert remains uncertain.

For this problem, based on regression analysis between LAI and climatic variables, we predicted the dynamic changes of vegetation in the later period (2013–2050). The adopted data included meteorological data, LAIs data (1982–2012), and five GCMs under three RCPs (2.6, 4.5, and 8.5) from the Fifth Phase of the Coupled Model Intercomparison Project (CMIP5) from 2013 to 2050. Our specific objectives are as follows: the first is to analyze variation of water and heat conditions including precipitation (P), temperature (T), and potential evapotranspiration (PET) from 1982 to 2012 and estimate their further variation (2013–2050) under various RCPs relative to 1982–2012; the second is to further explore spatiotemporal variation of LAI during 1982–2012 in the Mu Us Desert; the third objective is to predict the dynamic changes of LAIs (2013–2050) under the long-dated scenarios (2013–2050).

2. Research Data and Methods

2.1. Situation of the Research Area

We chose the Mu Us Desert as the research area which lies on 106°50′–111°30′ E longitude and 37°61′–40°22′ N latitude and covers approximately 4×10^4 km^2 (Figure 1). It is located in the transitional zone of arid and semi-arid, most of which belong to the continental monsoon climate [28], with an average annual temperature of 6.0–8.5 °C. The average annual precipitation is 250–440 mm, of which more than 60% occurs in summer. The present vegetation of research area is comprised of steppe or grassland, and the western margin belongs to the desertification steppe zone, the central and eastern parts belong to the typical grassland zone, and the southeast margin develops forest grassland. The major vegetation groups in this area are grassland, shrub, meadow, and marsh vegetation, chiefly dominated by *Stipabungeana*, *Artemisia frigida*, *Caragana korshinskii,* and *Carexstenophylla,* and so on [29]. There are various landscape types dominated by fixed, semi-fixed, or mobile dunes. In addition, grasslands and interconnected lakes and swamps are sporadically distributed [30]. The zonal soils consist of dark loessial soils, light chestnut soil, and brown soil, and the azonal soils are mainly sandy soils, meadow soils, and saline-alkali soils from east to west in this region [31]. It is noteworthy that there is a bedrock-dominated area in the northwest of the study area [32,33].

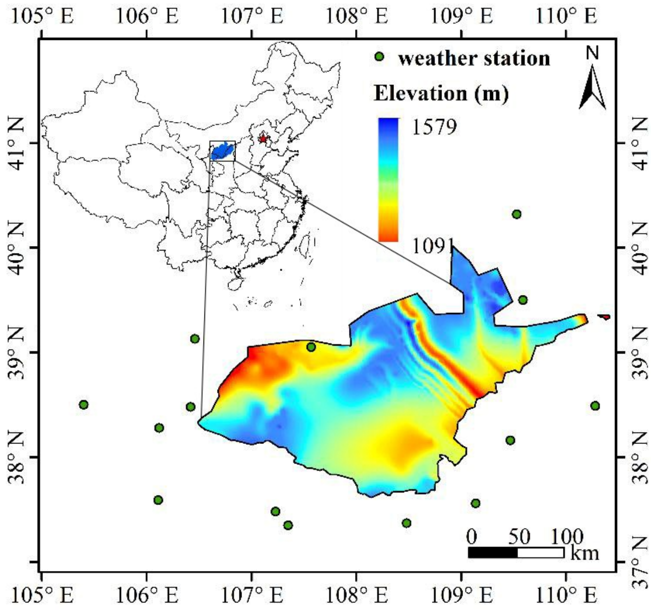

Figure 1. Mu Us Desert and meteorological stations location.

2.2. Data Source and Processing

All daily meteorological data including temperature, air pressure, relative humidity, wind speed, sunshine hours, and precipitation (mean, minimum, maximum) were obtained from 16 meteorological stations within and near the Mu Us Desert from China's National Meteorological Administration during the earlier period of 1982–2012. Then we interpolated the data onto a 0.083 grid covering the whole desert region using a thin plate smoothing spline method with the ANUSPLIN 4.3 software (Australian National university, Canberra, Australia) [34]. Moreover, 8-km re-sampling of the existing 90-m resolution digital elevation model (DEM) was developed by the Data Center for Resources and Environmental Sciences, Chinese Academy of Sciences (RESDC). The data of land use at a 1:100,000 scale in 2010 was also provided by RESDC.

The simulated climate projections from 1982–2050 were acquired from five GCMs (GFDL-ESM2M, HadGEM2-ES, IPSL-CM5A-LR, MIROC-ESM-CHEM, and NorESM1-M) under RCP 2.6, 4.5, and 8.5. The daily variables (the mean, maximum, and minimum temperatures (K); precipitation ($kg{\cdot}m^{-2}{\cdot}s^{-1}$); shortwave downwelling radiation ($W{\cdot}m^{-1}$); near-surface wind speed ($m{\cdot}s^{-1}$); and relative humidity (%)) of the GCMs were downscaled to 0.5, and the bias was corrected by the Inter-Sectoral Impact Model Intercomparison Project (ISI-MIP) [35,36].

The leaf area index (LAI) 15-daily temporal resolution data from the Mu Us Desert were obtained from the Global Land Surface Satellite (GLASS) LAI product because it provides temporally continuous profiles from 1982 to 2012 and is more accurate and of a higher quality than the CYCLOPES and MODIS LAI product with a 5-km spatial resolution in 1982–2000 and 1-km in 2001–2012 [37]. LAI has been chosen as the indicator of vegetation growth due to the understanding of broader biophysical and physiological processes, including photosynthesis, respiration, transpiration, carbon cycling, NPP, etc. [38,39].

2.3. Local Thin Plate Smoothing Spline Method

ANUSPLIN (Australian National university, Canberra, Australia) is based on the interpolation theory of ordinary thin plate and local thin plate spline function. Local thin plate smoothing spline method is an extension of thin plate smoothing spline prototype, which allows the introduction of a linear covariant quantum model in addition to the ordinary spline independent variables [40]. In this study, two modules, SPLINA and LAPGRD in the software, were used to interpolate meteorological factors, such as precipitation and temperature, with longitude and latitude as independent variables and altitude as covariables. The theoretical statistical model of local thin plate smoothing spline is:

$$z_i = f(x_i) + b^T y_i + e_i \qquad (i = 1, \ldots, N), \tag{1}$$

where, z_i is the dependent variable at point i in space, x_i is the independent variable of d dimensional spline, f is the unknown smoothing function of x_i, y_i is the independent covariant of p dimension, b is the p dimensional coefficient of y_i, e_i is the random error of independent variables with expected value 0 and variance $w_i\sigma^2$, where w_i is the known local relative variation coefficient as the weight, σ^2 is the error variance and is constant at all data points but usually unknown.

As can be seen from Equation (1), when the second term is missing in the equation, namely, when the covariant dimension p is 0, the model can be simplified as ordinary thin plate smoothing spline. When the first independent variable is missing, the model becomes a multiple linear regression model.

The functions f and b can be determined by least squares estimation:

$$\sum_{i=1}^{N} \frac{z_i - f(x_i) - b^T y_i}{w_i} + \rho J_m f(x) \tag{2}$$

where, J_m (f) is the roughness measure function of function $f(x_i)$, it is called the spline number, but also called roughness number in ANUSPLIN (Australian National university, Canberra, Australia). ρ is a positive smoothing parameter; it acts as a balance between data fidelity and surface roughness. ρ *is* usually determined by the minimization of generalized cross-validation (GCV) but also by minimization of the generalized maximum likelihood (GML) or expected true square error (MSE).

2.4. Potential Evapotranspiration (PET)

The Penman–Monteith model can be used to calculate daily reference evapotranspiration (PET_0 in mm·d^{-1}) then annual PET is obtained by summing all PET_0. The calculation formula is as follows and the calculation process of each component can be found in the literature [41].

$$PET_0 = \frac{0.408\Delta(R_n - G) + \gamma \frac{900}{T+273} u_2 (e_s - e_a)}{\Delta + \gamma(1 + 0.34u_2)} \tag{3}$$

where, Δ represents curve slope of saturation vapor pressure vs. air temperature (kPa °C^{-1}), R_n and G represent respectively net radiation and soil heat flux (MJ m^{-2} d^{-1}), γ represents psychometric constant, T represents average daily air temperature (°C), u_2 represents average daily wind speed at the 2-m height (m s^{-1}), e_s and e_a are, respectively, the saturation vapor pressure and actual vapor pressure (kPa).

2.5. Theil-Sen Trend Estimator

The linear regression analysis was used to detect the temporal and spatial variation of annual maximum LAI, average annual precipitation ($\overline{P}$), air temperature ($\overline{T}$) and PET in the Mu Us Desert. The overall trends of LAI and climatic variables were reflected by fitting a least squares regression through the time series of each pixel, and the trend slope coefficients were calculated [42], which is computed from:

$$Slope = \frac{n \sum_{i=1}^{n} i \cdot x_i - \sum_{i=1}^{n} i \sum_{i=1}^{n} x_i}{n \sum_{i=1}^{n} i^2 - \left(\sum_{i=1}^{n} i\right)^2} \tag{4}$$

where, *slope* represents the average change rate (i.e., trend) of the time-series data. n is the cumulative years during the study period, and i is the year serial number. x_i represents a dependent variable (i.e., LAI, precipitation (P), air temperature (T), or PET) for year i.

These correlation coefficients between LAI and other climate variables (i.e., P, T, or PET) can be calculated by using the Pearson correlation method. We have checked the data before using linear regression and Pearson correlation to be sure that all data have a normal distribution.

3. Result Analysis

3.1. Climatic Variables

To check the performance of simulated values of climatic variables from 2013–2050 in the Mu Us Desert, the linear regression analysis was performed for the fitting of the data between the simulated annual values and corresponding observational values during the earlier period (1982–2012). The fitting results (Figure 2) showed that: the coefficients of determination (R^2) demonstrated the simulations and observations generally agreed with R^2 of 0.6463 and 0.5786 for $\overline{P}$ and $\overline{T}$, respectively. This indicated that the later climate prediction data using the above-obtained linear regression equation could achieve good results and have the rationality and credibility of application.

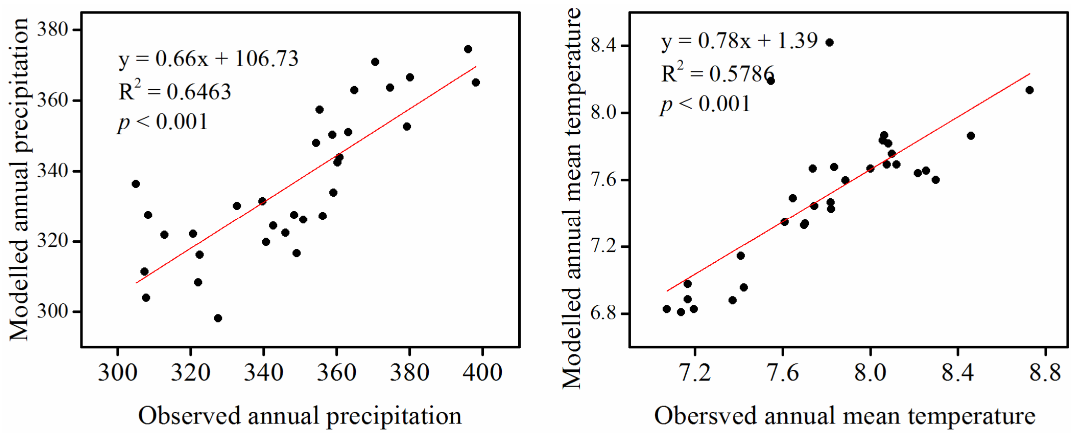

Figure 2. Comparison of the observed and simulated annual values during 1982–2012.

Figure 3 showed the spatial distributions of the long series $\overline{P}$, $\overline{T}$, and PET during the observed period and RCP 4.5 scenario (RCP 2.6 and RCP 8.5 scenarios were omitted) in the Mu Us Desert. The distributions of $\overline{P}$ exhibited similar spatial patterns during the observed period and all RCP scenarios, and had a gradually decreasing from east to west with the range of 198.4–383.6 mm, 218.6–427 mm, 218.1–422 mm, and 215.4–422.3 mm for the earlier period and three RCPs (2.6, 4.5, and 8.5) in the Mu Us Desert (Figure 3a,b). The spatial patterns of $\overline{T}$ were not uniform between observations and scenarios, but were similar for three RCPs scenarios, with the range of 5.7–9.2 °C, 7.7–10.2 °C, 7.6–10.1 °C, and 7.9–10.4 °C for the observed period and all RCP scenarios, respectively (Figure 3c,d). The spatial distributions of annual PET were similar during the observed period and all scenarios, and had a gradual increase from east to west with the range of 942.6–1110.4 mm, 1095.7–1226.7 mm, 1084.5–1224.2 mm, and 1093.4–1230.8 mm in the Mu Us Desert for the observed period and all the RCP scenarios, respectively (Figure 3e,f).

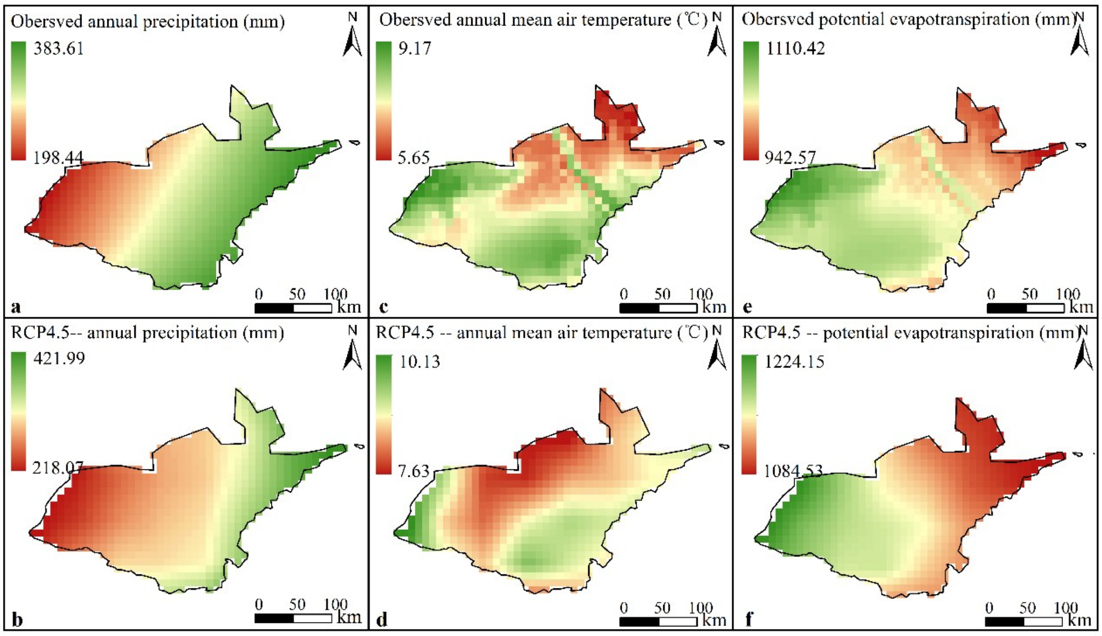

Figure 3. The spatial distributions of the long series annual precipitation ($\overline{P}$), air temperature ($\overline{T}$), and potential evapotranspiration (PET) during the observed period and representative concentration pathways (RCP) 4.5 scenario in the Mu Us desert.

Figure 4 showed the change process of annual precipitation, air temperature, and the PET time series of the observed spatial mean values for the earlier observed period (1982–2012) and the simulated spatial mean values for the later period (2013–2050) using the 10-year running mean in the Mu Us Desert. Figure 4a provided the time series of observed and simulated regional mean values of annual precipitation. The results indicated annual fluctuation and an increasing trend in precipitation during the observed period, and the change rate of 0.6 mm·yr^{-1} ($p \geq 0.05$). The increasing trend in precipitation was captured in all scenarios in the Mu Us Desert (Table 1). Comparing the observed precipitation during the earlier period with the result of the five-GCM ensemble mean during 2013–2050 under the three RCPs, precipitation changes were uniform between observations and scenarios, yet the change magnitude of precipitation was different under the three RCPs. The annual precipitation slightly rose by 9.8%, 11.0%, and 10.6% by 2050 under the three RCPs contrasting the precipitation during the observed period (Table 1). The time series of regional mean values of annual air temperature was presented in Figure 4b. A warming trend occurred during the earlier period ($p < 0.01$) and it is expected that the average annual temperature will continue to warm in the later period ($p < 0.01$, Table 1) in the Mu Us Desert. Compared with the observations, the simulated temperature increased with most strong changes for RCP 8.5 and smallest magnitudes for RCP 2.6. Relative to the observation period, the annual temperature rose respectively by 0.60 °C, 0.69 °C, and 0.97 °C by 2050 under the three RCPs (Table 1). Figure 4c showed a time series of observed and simulated regional mean values of annual PET. The results revealed that an increasing trend in PET has appeared during the earlier period ($p < 0.05$) and were projected to persist into the later period under each RCP ($p < 0.01$, Table 1). Comparing the observed values during the earlier period with the results of the five-GCM ensemble mean, PET rose respectively by 7.3%, 6.5%, and 7.0% under three RCPs (Table 1).

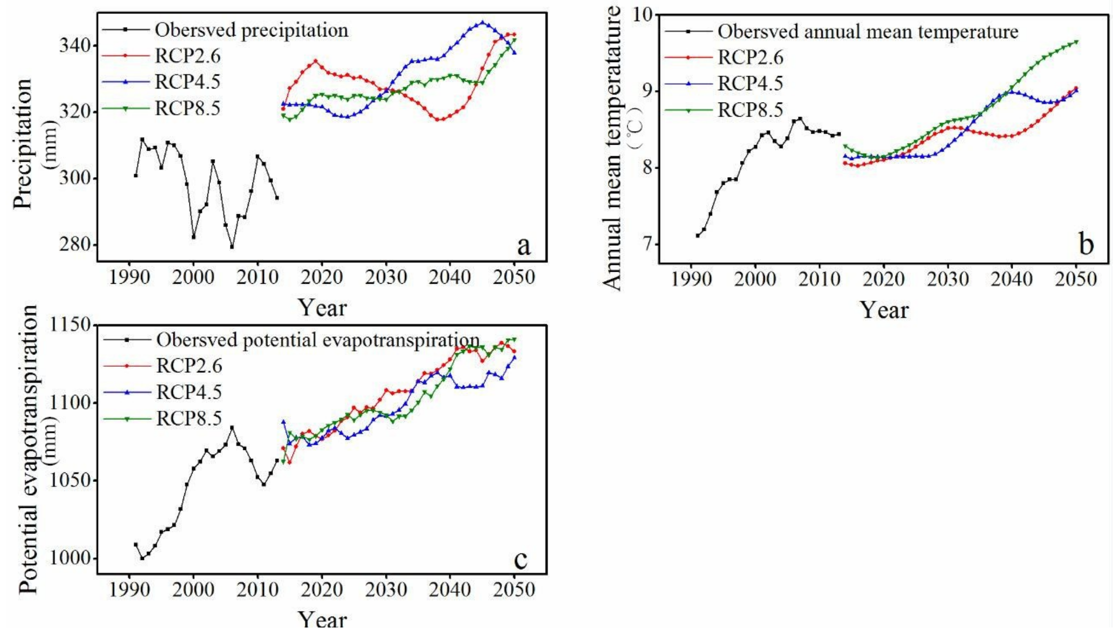

Figure 4. Changes of observed and simulated regional mean values of annual precipitation (**a**), air temperature (**b**), and PET (**c**) in the Mu Us Desert.

Table 1. The regional mean values and the trends of annual precipitation, air temperature, and PET in Mu Us Desert.

Period	*P* (mm)	*P*-trend (mm·yr^{-1})	*T* (°C)	*T*-trend (°C·yr^{-1})	*PET* (mm)	*PET*-trend (mm·yr^{-1})
1982–2012	299.26	0.60	7.96	**0.049 ****	1038.92	**1.67 ***
RCP 2.6	328.45	**0.37 ***	8.55	**0.026 ****	1114.37	**1.90 ****
RCP 4.5	332.06	**0.54 ****	8.65	**0.032 ****	1106.10	**2.00 ****
RCP 8.5	331.00	**0.66 ****	8.92	**0.045 ****	1111.71	**2.02 ****

Note: *and ** denote respectively statistically significant trend of $p < 0.05$ and $p < 0.01$.

3.2. Vegetation Dynamics

There are various types of land use (e.g., farmland, urbanization, and water bodies) in the study area where the desert is not completely covered. To accurately explore the characteristics of spatiotemporal vegetation variation and its inherent relationship with climate change, the above-mentioned types of land use were excluded from the analysis.

Spatial distribution of the over years mean from 1982–2012 in annual maximum of LAI reflected the general situation of vegetation growth, and the value range of annual maximum LAI was 0.4–0.9 m^2·m^{-2} (Figure 5a). The value between 0.6–0.8 and 0.4–0.6 m^2·m^{-2} was the main body, and occupied 64.4% and 30.8% of the whole area, respectively, with the higher values of LAI occurring in the south and the lower values in the northwest of the study area.

In the whole study area, annual maximum LAI derived from GLASS was on the rise with the change rate of 0.029 m^2 m^{-2} yr^{-1} ($p < 0.05$). The area with increasing trend occupied 84.9% of the whole area, while the vegetation growth status was mainly slight, and significant improvements were found with 83.3% and 1.6% of the total area, respectively (Table 2). Furthermore, vegetation exhibited stability or a decreasing trend in some scattered areas of the Mu Us Desert (Figure 5b).

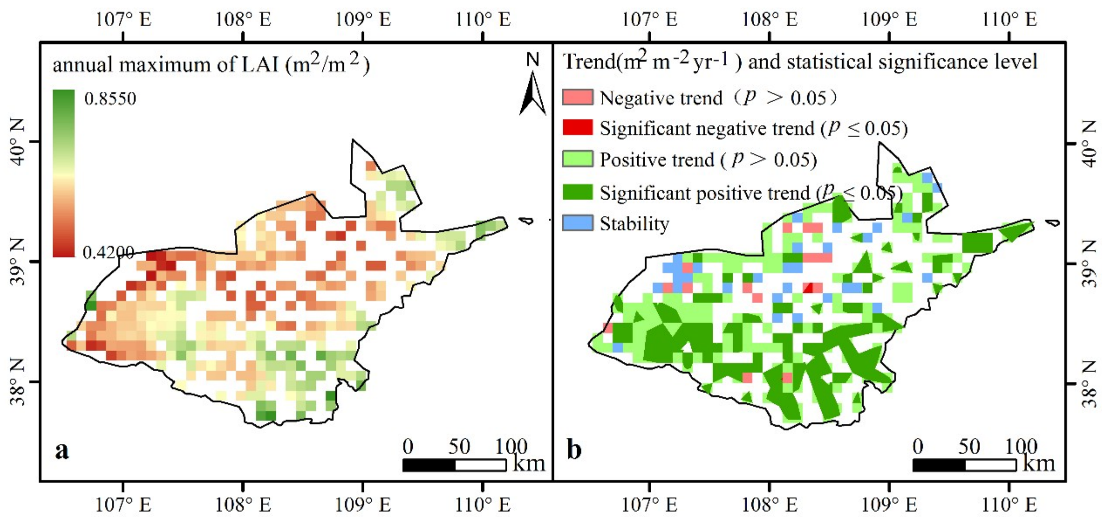

Figure 5. The spatial distribution and time trend of the over years mean (1982–2012) in the annual maximum of leaf area index (LAI) in the Mu Us Desert.

Table 2. Trend and variation classification of annual maximum LAI during 1982–2012.

Classification of Variation	Trend	Area Percentage (%)
Serious degradation	$Slope \leq -0.01$	/
Slight degradation	$-0.01 < Slope \leq -0.0006$	5.1
Stability	$-0.0006 < Slope \leq 0.0006$	9.9
Slight improvement	$0.0006 < Slope \leq 0.01$	83.4
Significant improvement	$Slope > 0.01$	1.6

3.3. Correlation Analysis between LAI and Climatic Variables

By correlation analysis, we calculated the correlation coefficients between annual maximum LAI and climatic variables (Table 3). The results revealed the significant correlation between annual maximum LAI and precipitation (P), the correlation coefficient was 0.567 ($p < 0.01$). However, LAI was negatively correlated with temperature (T) and PET, and the correlation between LAI and PET was higher than that between LAI and temperature. Furthermore, LAI was also related to terrain factors such as DEM, longitude, and latitude. LAI was negatively correlated with DEM ($p < 0.01$) and positively correlated with longitude ($p < 0.01$), but there was no significant relationship between LAI and latitude ($p \geq 0.05$).

Table 3. Correlation coefficients between annual maximum LAI and climatic variables.

Variables	Correlation Coefficient	Variables	Correlation Coefficient
P	**0.567** **	*DEM*	**−0.237** **
T	−0.197	*Longitude*	**0.349** *
PET	**−0.373** **	*Latitude*	−0.065

Note: * and ** denote respectively significant correlation at 5% and 1% level (2-tailed).

3.4. Possible LAIs under Three Scenarios

According to the correlation coefficients in Table 3, we selected the main factors affecting vegetation growth, including precipitation, PET, longitude, and DEM. Based on regression analysis, we quantified the relationship between annual maximum LAI and other relevant variables. The corresponding regression equation was as follows:

$$LAI = 0.002523P - 0.000305PET - 0.001092Longitude + 0.000056DEM + 0.220101 \; (R^2 = 0.683, p < 0.01) \quad (5)$$

Based on the five-GCM ensemble mean in three RCPs, we predicted the LAI in the later period (2013–2050). The LAIs by 2050 were respectively 0.42–0.88 $m^2 \cdot m^{-2}$, 0.42–0.87$m^2 \cdot m^{-2}$, and 0.41–0.87$m^2 \cdot m^{-2}$ under the three RCPs (Table 4). Compared with the annual maximum LAI in the earlier period (1982–2012), LAI was found to be already close to the current situation in the northwestern and southern parts of the study area (Figure 6).

Table 4. The long-dated LAI and its change magnitude.

Period	1982–2012 ($m^2 \cdot m^{-2}$)	RCP 2.6 ($m^2 \cdot m^{-2}$)	RCP 4.5 ($m^2 \cdot m^{-2}$)	RCP 8.5 ($m^2 \cdot m^{-2}$)
LAI	0.4200–0.8550	0.4200–0.8825	0.4189–0.8728	0.4121–0.8739
Magnitude	-	−0.0412–0.2768	−0.0421–0.2614	−0.0484–0.2647

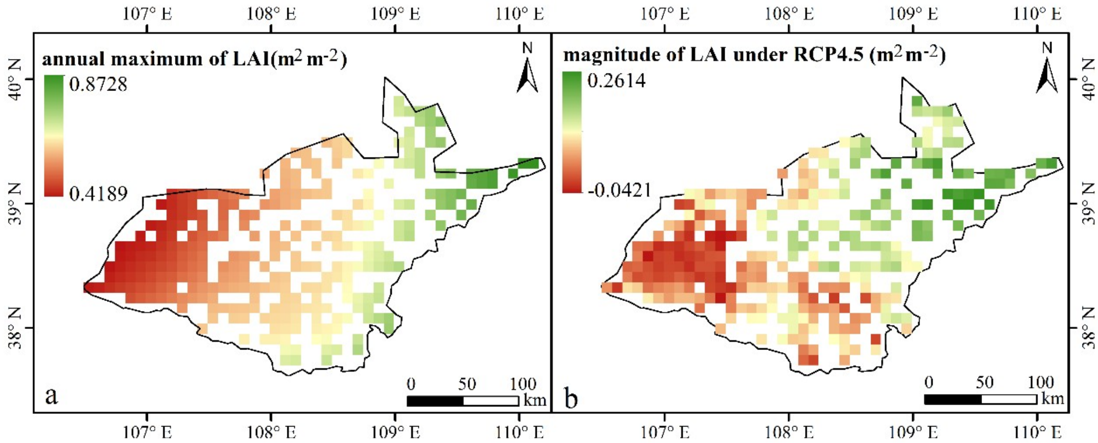

Figure 6. Spatial distribution of average values (**a**) and change magnitude (**b**) in annual maximum of LAI during 2013–2050 under RCP 4.5 scenario in the Mu Us Desert.

4. Discussion

4.1. Change on Climatic Variables

According to the data of IPCC [43], climate change together with anthropogenic emissions of greenhouse gases has caused the global near-surface temperature rose by 0.7 °C from 1951 to 2012, amounting to an increase with a rate-of-change of 0.01 °C yr^{-1}. This research presented that the impact of global climate change had led to a greater temperature rise in the Mu Us Desert, averaging to about 0.049 °C yr^{-1} increase during 1982–2012 (Table 1). This increased rate reached 4.9 times greater than the global level. Li et al. (2015) [44] also reported a strong uptrend in temperature in most drylands of China during 1948–2008 (0–0.1 °C yr^{-1} increases), except for several small scattered patches (−0.02–0 $°C \cdot yr^{-1}$ decreases). From Table 1, we can conclude that the warming trends were projected to persist into the long-dated and, respectively, rose by 0.6 °C, 0.7 °C, and 1 °C by 2050 for the three RCPs. Based on the five identical GCMs ensemble means, Yin et al. (2015) [45] reported that annual surface temperature in China would respectively rise by 1.8 °C, 2.2 °C, and 2.8 °C by 2050 for three RCPs corresponding to the data during 1981–2010. However, long-dated warming magnitude in the Mu Us Desert was lower than that of China in this study. In addition, precipitation and PET are projected to increase substantially for all RCPs in China. Our study showed that similar increases were detected in precipitation and PET for all RCPs by 2050 in the Mu Us Desert.

4.2. Vegetation Dynamics and Correlation with Climatic Variables

At the global scale, change analysis of observed maximum LAI showed to greening [46]. By means of analyzing inter-annual variability of maximum LAI in the Mu Us Desert during the past 31 years, changes in LAI exhibited a similar widespread greening trend with slight and significant improvement (Figure 5b). Our results indicated that regional vegetation had been improved in the Mu Us Desert.

In drylands, climate change but especially precipitation has a great influence on vegetation growth and development [47–49]. In this study, we found that the changes of LAI were highly correlated with precipitation variations, indicating that precipitation was a major climatic element of vegetation activities in the Mu Us Desert. Previous studies suggested that the warming trend in the earlier period could exacerbate desertification in desert ecosystems [50]. Nevertheless, this study showed that there was no significant correlation between LAI and temperature, yet there was a significant negative correlation with PET in the Mu Us Desert (Table 3).

4.3. Correlation of Vegetation and Ecological Restoration Activities

Given the massive afforestation and re-vegetation programs during the last decade and planning afforestation and re-vegetation programs ending in 2050 [19,51,52], it is important to recognize that an over-reliance on afforestation to rebuild desert ecosystems may lead to water shortages that could result in failure [19,53]. Therefore, under this backdrop, knowing the long-dated dynamic changes of vegetation is critical for ensuring sustainable development in the vulnerable desert environment. Research results indicated that compared with the present data (1982–2012), the annual maximum of LAI by 2050 was already close to the current value in the northwest and south of this study region. This study suggested that we should consider the permissible maximum critical value of vegetation when the planning for long-dated restoration programs would be carried out in this region. That may prevent excessive restoration from resulting in impoverished lands with few ecological and economic benefits [54].

4.4. Uncertainty

Although the GLASS LAI can provide a high-quality temporally continuous dataset, the accuracy of the dataset is limited and uncertain in the Mu Us Desert, which needs to be further verified. In order to assess climate model performance and reduce the uncertainty of GCMs performance, the five-GCM ensemble mean was used, and the earlier simulations were compared with observations during the observed period. Validation of simulated precipitation and temperature in 1982–2012 showed that the patterns of two variables were usually similar between simulations and observations in the Mu Us Desert. Though the simulated results can be improved by the correction method, the improvement is limited and a number of uncertainties remain because the correction method was based on the statistical mapping relationship between observation and simulation. Furthermore, these low regression coefficients of the LAI and climatic variables, terrain (R^2 = 0.683) indicated considerable uncertainties in the regression model. There are some other factors (sunshine, wind speed, and human activities, etc.) should not be neglected in detecting the spatial distribution pattern of vegetation. It cannot be ignored that spatial autocorrelation had a great influence on the global regression analysis so it may not get better estimation results. It is necessary to find a suitable statistical method that addresses spatial autocorrelation and the corresponding errors in the following study.

5. Conclusions

Based on regression analysis between LAI and some climatic variables in the Mu Us Desert, we developed a method to determine the long-dated LAIs that could show the vegetation dynamics and climate change responses as well as the mechanisms of these vegetation dynamics. Our study suggested that the ecological environment had been improved in the Mu Us Desert and the permissible LAIs by 2050 were, respectively, 0.42–0.88$m^2 \cdot m^{-2}$, 0.42–0.87$m^2 \cdot m^{-2}$, 0.41–0.87$m^2 \cdot m^{-2}$ under the three RCPs. Knowing long-dated possible LAI is important for implementing current and planned ecological restoration. Compared with the baseline period (1982–2012), LAIs were found to be already close to current values in the northwestern and southern Mu Us Desert. Based on the vegetation dynamics and the responses under climate change in the Mu Us Desert, it is necessary to research the “threshold” of key attributes of ecosystems (such as water carrying capacity of vegetation) in long-dated ecological restoration and reconstruction projects and to strengthen the management and allocation of water resources further. That may avoid the excessive restoration leading to contradictions of water utilization between the ecosystem and human.

Author Contributions: D.Z. and Y.S. designed the study of the paper, contributed to the ideas, interpretation of the data, and manuscript writing; Y.W. contributed to data processing and manuscript modifying; L.W. contributed to data processing and analysis. All authors contributed to the discussion and commented on the manuscript at all stages.

Funding: This research was funded by the National Social Science Foundation of China (Grant No. 17BJL105).

Conflicts of Interest: The authors declare no conflict of interest.

References

1. Lioubimtseva, E. A multi-scale assessment of human vulnerability to climate change in the Aral Sea Basin. *Environ. Earth Sci.* **2015**, *73*, 719–729. [CrossRef]
2. Chen, L.; Wei, W.; Fu, B.; Lü, Y. Soil and water conservation on the Loess Plateau in China: Review and perspective. *Prog. Phys. Geogr.* **2007**, *31*, 389–403. [CrossRef]
3. Mohammad, A.G.; Adam, M.A. The impact of vegetative cover type on runoff and soil erosion under different land uses. *Catena* **2010**, *81*, 97–103. [CrossRef]
4. Zhu, L.Q.; Zhu, W.B. Research on effects of land use/cover change on soil erosion. *Adv. Mater. Res.* **2012**, *433*, 1038–1043. [CrossRef]
5. Zhang, X.P.; Zhang, L.; McVicar, T.R.; Van Niel, T.G.; Li, L.T.; Li, R.; Yang, Q.K.; Wei, L. Modelling the impact of afforestation on average annual streamflow in the Loess Plateau, China. *Hydrol. Process.* **2008**, *22*, 1996–2004. [CrossRef]
6. Xin, Z.; Yu, X.; Lu, X.X. Factors controlling sediment yield in China's Loess Plateau. *Earth Surf. Process. Landf.* **2011**, *36*, 816–826. [CrossRef]
7. Dregne, H.E. Arid land degradation-a result of mismanagement. *Geotimes* **1991**, *36*, 19–21.
8. Dregne, H.E. Land degradation in the drylands. *Arid Soil Res. Rehabil.* **2002**, *16*, 99–132. [CrossRef]
9. Le Houérou, H.N. Restoration and rehabilitation of arid and semiarid Mediterranean ecosystems in North Africa and West Asia: A review. *Arid Soil Res. Rehabil.* **2000**, *14*, 3–14. [CrossRef]
10. Durán, O.; Herrmann, H.J. Vegetation against dune mobility. *Phys. Rev. Lett.* **2006**, *97*, 188001. [CrossRef]
11. Feng, X.; Fu, B.; Lu, N.; Zeng, Y.; Wu, B. How ecological restoration alters ecosystem services: An analysis of carbon sequestration in China's Loess Plateau. *Sci. Rep.* **2013**, *3*, 2846. [CrossRef]
12. Wang, S.; Fu, B.; Piao, S.; Lü, Y.; Ciais, P.; Feng, X.; Wang, Y. Reduced sediment transport in the Yellow River due to anthropogenic changes. *Nat. Geosci.* **2016**, *9*, 38–41. [CrossRef]
13. Lü, Y.; Fu, B.; Feng, X.; Zeng, Y.; Liu, Y.; Chang, R.; Sun, G.; Wu, B. A policy-driven large scale ecological restoration: Quantifying ecosystem services changes in the Loess Plateau of China. *PLoS ONE* **2012**, *7*, e31782. [CrossRef]
14. Wang, G.; Innes, J.L.; Lei, J.; Dai, S.; Wu, S.W. China's forestry reforms. *Science* **2007**, *318*, 1556–1557. [CrossRef] [PubMed]
15. State Forestry Administration P.R. China. *A Bulletin of Status Quo of Desertification and Sandification in China*; China Water Power Press: Beijing, China, 2011; p. 22.
16. Li, X.R.; Zhang, Z.S.; Huang, L.; Wang, X. Review of the ecohydrological processes and feedback mechanisms controlling sand-binding vegetation systems in sandy desert regions of China. *Chin. Sci. Bull.* **2013**, *58*, 1483–1496. [CrossRef]
17. Mu, X.M.; Xu, X.X.; Wang, W.L.; Weng, Z.M.; Du, F. Impact of artificial. *Acta Pedol. Sin.* **2003**, *2*, 210–217.
18. Guo, K.; Dong, X.J.; Liu, Z.M. Characteristics of soil moisture content on sand dunes in Mu Us sandy grassland why artemisia ordosica declines on old fixed sand dunes. *Acta Phytoecol. Sin.* **2000**, *3*, 275–279.
19. Feng, X.; Fu, B.; Piao, S.; Wang, S.; Ciais, P.; Zeng, Z.; Lü, Y.; Zeng, Y.; Li, Y.; Jiang, X.; et al. Revegetation in China's Loess Plateau is approaching sustainable water resource limits. *Nat. Clim. Chang.* **2016**, *6*, 1019–1022. [CrossRef]
20. Guo, Z.S.; Shao, M.A. Soil water carrying capacity of vegetation and soil desiccation in artificial forestry and grassland in semi-arid regions of the Loess Plateau. *Acta Ecol. Sin.* **2003**, *23*, 1640–1647.

21. Xia, Y.Q.; Shao, M.A. Soil water carrying capacity for vegetation: A hydrologic and biogeochemical process model solution. *Ecol. Model.* **2008**, *214*, 112–124. [CrossRef]
22. Correa-Tedesco, G.; Rousseaux, M.C.; Searles, P.S. Plant growth and yield responses in olive (*Olea europaea*) to different irrigation levels in an arid region of Argentina. *Agric. Water Manag.* **2010**, *97*, 1829–1837. [CrossRef]
23. Li, X.; Zhang, Z.; Tan, H.; Gao, Y.; Liu, L.; Wang, X. Ecological restoration and recovery in the wind-blown sand hazard areas of northern China: Relationship between soil water and carrying capacity for vegetation in the Tengger Desert. *Sci. China Life Sci.* **2014**, *57*, 539. [CrossRef] [PubMed]
24. Liu, B.; Shao, M. Modeling soil–water dynamics and soil–water carrying capacity for vegetation on the Loess Plateau. *Agric. Water Manag.* **2015**, *159*, 176–184. [CrossRef]
25. Lioubimtseva, E.; Henebry, G.M. Climate and environmental change in arid Central Asia: Impacts, vulnerability, and adaptations. *J. Arid Environ.* **2009**, *73*, 963–977. [CrossRef]
26. Liu, J.; Li, S.; Ouyang, Z.; Tam, C.; Chen, X. Ecological and socioeconomic effects of China's policies for ecosystem services. *Proc. Natl. Acad. Sci. USA* **2008**, *105*, 9477–9482. [CrossRef] [PubMed]
27. Li, Y.C. Grain for Green program is a great concrete action towards the ecological civilization in China: Summary of a decade program implementation. *For. Constr.* **2009**, *27*, 3–13.
28. Liu, X.; Lu, R.; Lü, Z.; Du, J.; Jia, F.; Li, T.; Chen, L.; Wu, Y. Magnetic susceptibility of surface soils in the Mu Us Desert and its environmental significance. *Aeolian Res.* **2017**, *25*, 127–134. [CrossRef]
29. Liu, B.; Jin, H.L.; Sun, L.Y.; Sun, Z.; Niu, Q.H.; Zhang, C.X. Geochemical characteristics of Holocene aeolian deposits and their environmental significance in the Mu Us desert, northern China. *Geol. J.* **2016**, *51*, 325–337. [CrossRef]
30. Zhou, W.J.; Donahue, D.J.; Porter, S.C.; Jull, T.A.; Li, X.Q.; Stuiver, M.; An, Z.S.; Matsumoto, E.; Dong, G.R. Variability of Monsoon Climate in East Asia at the End of the Last Glaciation. *Quat. Res.* **1996**, *46*, 219–229.
31. Liu, B.; Jin, H.; Sun, L.; Sun, Z.; Niu, Q.; Xie, S.; Li, G. Holocene moisture change revealed by the Rb/Sr ratio of aeolian deposits in the southeastern Mu Us Desert, China. *Aeolian Res.* **2014**, *13*, 109–119. [CrossRef]
32. Kapp, P.; Pullen, A.; Pelletier, J.D.; Russell, J.; Goodman, P.; Cai, F. From dust to dust: Quaternary wind erosion of the Mu Us Desert and Loess Plateau, China. *Geology* **2015**, *43*, 835–838. [CrossRef]
33. Yue, L.P.; Li, J.X.; Zheng, G.Z.; Li, Z. Evolution of the Ordos Plateau and environmental effects. *Sci. China Ser. D Earth Sci.* **2007**, *50*, 19–26. [CrossRef]
34. Hutchinson, M.F. ANUSPLIN Version 4.3 User Guide. Canberra: The Australia National University, Center for Resource and Environment Studies. 2004. Available online: http://cres.anu.edu.au/outputs/anusplin.Php (accessed on 15 December 2017).
35. Hempel, S.; Frieler, K.; Warszawski, L.; Schewe, J.; Piontek, F. A trend-preserving bias correction–the ISI-MIP approach. *Earth Syst. Dyn.* **2013**, *4*, 219–236. [CrossRef]
36. Warszawski, L.; Frieler, K.; Huber, V.; Piontek, F.; Serdeczny, O.; Schewe, J. The inter-sectoral impact model intercomparison project (ISI–MIP): Project framework. *Proc. Natl. Acad. Sci. USA* **2014**, *111*, 3228–3232. [CrossRef] [PubMed]
37. Liang, S.; Zhao, X.; Liu, S.; Yuan, W.; Cheng, X.; Xiao, Z.; Zhang, X.; Liu, Q.; Cheng, J.; Tang, H.; et al. A long-term Global LAnd Surface Satellite (GLASS) data-set for environmental studies. *Int. J. Digit. Earth* **2013**, *6*, 5–33. [CrossRef]
38. Jonckheere, I.; Fleck, S.; Nackaerts, K.; Muys, B.; Coppin, P.; Weiss, M.; Baret, F. Review of methods for in situ leaf area index determination: Part I. Theories, sensors and hemispherical photography. *Agric. For. Meteorol.* **2004**, *121*, 19–35. [CrossRef]
39. Hardin, P.J.; Jensen, R.R. The effect of urban leaf area on summertime urban surface kinetic temperatures: A Terre Haute case study. *Urban For. Urban Green.* **2007**, *6*, 63–72. [CrossRef]
40. Qian, Y.L.; Lv, H.Q.; Zhang, Y.H. Application and assessment of spatial interpolation method on daily meteorological elements based on ANUSPLIN software. *J. Meteorol. Environ.* **2010**, *26*, 7–15.
41. Allen, R.G.; Pereira, L.S.; Raes, D.; Smith, M. *Crop Evapotranspiration-Guidelines for Computing Crop Water Requirements-FAO Irrigation and Drainage Paper 56*; FAO: Rome, Italy, 1998; Volume 300, p. D05109.
42. Jiapaer, G.; Liang, S.; Yi, Q.; Liu, J. Vegetation dynamics and responses to recent climate change in Xinjiang using leaf area index as an indicator. *Ecol. Indic.* **2015**, *58*, 64–76.

43. Stocker, T.F.; Qin, D.; Plattner, G.K.; Tignor, M.M.B.; Allen, S.K.; Boschung, J.; Nauels, A.; Xia, Y.; Bex, V.; Midgley, P.M. *Climate Change 2013: The Physical Science Basis. Contribution of Working Group I to the Fifth Assessment Report of IPCC the Intergovernmental Panel on Climate Change*; Cambridge University Press: Cambridge, UK, 2014. [CrossRef]
44. Li, Y.; Huang, J.; Ji, M.; Ran, J. Dryland expansion in northern China from 1948 to 2008. *Adv. Atmos. Sci.* **2015**, *32*, 870–876. [CrossRef]
45. Yin, Y.; Ma, D.; Wu, S.; Pan, T. Projections of aridity and its regional variability over China in the mid-21st century. *Int. J. Climatol.* **2015**, *35*, 4387–4398. [CrossRef]
46. Zhu, Z.; Piao, S.; Myneni, R.B.; Huang, M.; Zeng, Z.; Canadell, J.G.; Ciais, P.; Sitch, S.; Friedlingstein, P.; Arneth, A.; et al. Greening of the Earth and its drivers. *Nat. Clim. Chang.* **2016**, *6*, 791–795. [CrossRef]
47. Nicholson, S.E.; Farrar, T.J. The influence of soil type on the relationships between NDVI, rainfall, and soil moisture in semiarid Botswana. Part I. NDVI response to rainfall. *Remote Sens. Environ.* **1994**, *50*, 107–120. [CrossRef]
48. Wang, J.; Price, K.P.; Rich, P.M. Spatial patterns of NDVI in response to precipitation and temperature in the central Great Plains. *Int. J. Remote Sens.* **2001**, *22*, 3827–3844. [CrossRef]
49. Zhang, J.T.; Ru, W.; Li, B. Relationships between vegetation and climate on the Loess Plateau in China. *Folia Geobot.* **2006**, *41*, 151–163. [CrossRef]
50. Yang, X.; Ding, Z.; Fan, X.; Zhou, Z.; Ma, N. Processes and mechanisms of desertification in northern China during the last 30 years, with a special reference to the Hunshandake Sandy Land, eastern Inner Mongolia. *Catena* **2007**, *71*, 2–12. [CrossRef]
51. Lal, R. Potential of desertification control to sequester carbon and mitigate the greenhouse effect. *Clim. Chang.* **2001**, *51*, 35–72. [CrossRef]
52. Lal, R. Carbon sequestration in dryland ecosystems. *Environ. Manag.* **2004**, *33*, 528–544. [CrossRef]
53. Sun, W.; Song, X.; Mu, X.; Gao, P.; Wang, F.; Zhao, G. Spatiotemporal vegetation cover variations associated with climate change and ecological restoration in the Loess Plateau. *Agric. For. Meteorol.* **2015**, *209*, 87–99. [CrossRef]
54. Bourque, C.P.A.; Meng, F.R.; Gullison, J.J. Biophysical and potential vegetation growth surfaces for a small watershed in northern Cape Breton Island, Nova Scotia, Canada. *Can. J. For. Res.* **2000**, *30*, 1179–1195. [CrossRef]